Transport Implications Resulting from Internal Redistribution of Arsenic and Iron within Constructed Soil Aggregates

YOKO MASUE-SLOWEY,[†]
BENJAMIN D. KOCAR,[†]
SERGIO ANDRÉS BEA JOFRÉ,[‡]
K. ULRICH MAYER,[‡] AND
SCOTT FENDORF*,[†]

Department of Environmental Earth System Sciences, Stanford University, Stanford, California, United States, and Department of Earth and Ocean Sciences, The University of British Columbia, Vancouver, British Columbia, Canada

Soils are an aggregate-based structured media that have a multitude of pore domains resulting in varying degrees of advective and diffusive solute and gas transport. Consequently, a spectrum of biogeochemical processes may function at the aggregate scale that collectively, and coupled with solute transport, determine element cycling in soils and sediments. To explore how the physical structure impacts biogeochemical processes influencing the fate and transport of As, we examined temporal changes in speciation and distribution of As and Fe within constructed aggregates through experimental measurement and reactive transport simulations. Spherical aggregates were made with As(V)-bearing ferrihydrite-coated sand inoculated with *Shewanella* sp. ANA-3; aerated solute flow around the aggregate was then induced. Despite the aerated aggregate exterior, where As(V) and ferrihydrite persist as the dominant species, anoxia develops within the aggregate interior. As a result, As and Fe redox gradients emerge, and the proportion of As(III) and magnetite increases toward the aggregate interior. Arsenic(III) and Fe(II) produced in the interior migrate toward the aggregated exterior and result in coaccumulation of As and Fe(III) proximal to preferential flow paths as a consequence of oxygenic precipitation. The oxidized rind of aggregates thus serves as a barrier to As release into advecting pore-water, but also leads to be a buildup of this hazardous element at preferential flow boundaries that could be released upon shifting geochemical conditions.

Introduction

Arsenic has an extensive legacy as a human toxin and is commonly found in water and soil from both geological and anthropogenic sources (*1*). In soils and waters, As commonly resides in the inorganic As(V) or As(III) species. Dissolved concentrations of As are typically regulated by adsorption on mineral surfaces (*1*). Arsenic(V) has an affinity for a range of minerals (*1–4*), while, conversely, appreciable As(III)

adsorption is generally limited to Fe (hydr)oxides (*2–4*). In most soil environments, reduction of As(V) and Fe(III) are considered the most ubiquitous mechanisms controlling As desorption (*1*); redox transformations of As and Fe are largely microbially mediated, and a diverse array of As(V) and Fe(III) reducing microorganisms have been isolated (*5, 6*).

Arsenic(V) reduction to As(III) can stimulate desorption despite the higher adsorption maxima of As(III) on Fe (hydr)oxides at circum-neutral and greater pH (*7–9*). Additionally, reductive dissolution and transformation of Fe (hydr)oxides such as ferrihydrite are often purported to induce As desorption. However, recent evidence illustrates that either release or transient sequestration of As can result from ferrihydrite reduction owing to the formation of secondary phases that scavenge As (*10–13*). Under sustained anaerobic conditions, ferrihydrite reduction could lead to a dual-stage process where As is initially retained during ferrihydrite transformation and subsequently released during dissolution of the secondary Fe minerals. The sequestration period depends on ferrihydrite transformation to secondary (hydr)oxides and reaction conditions.

A multitude of biogeochemical processes may therefore impact the fate of As and, as a consequence of the physical complexity within soils, they may vary at the submicrometer scale (*14*). Soils are structured media having a multitude of pore-domains that result in advective and diffusively controlled solute transport. Solutes move rapidly via advection along preferential flow paths (e.g., aggregate exteriors) and slowly via diffusion into intra-aggregate pore space. As a consequence primarily of diffusion limited oxygen egress, combined with biological demand, aggregate interiors are typically more chemically reducing than exterior regions—even in aerated soils, aggregates may become reducing within a few millimeters of the exterior (*15*). Such a variation in redox status within aggregates may result in a diversity of operative respiratory pathways. Despite being seemingly well aerated, anaerobic metabolisms such as denitrification (*15*) and methanogenesis (*16*) are observed, and As(V) and Fe(III) reduction should not be exceptions. However, the consequence of intra-aggregate As(V) and Fe(III) reduction processes that ultimately combine to control the fate of As within aerated, structured soils is unknown. Accordingly, the goal of this study was to decipher the temporal changes in speciation and distribution of As and Fe, along with the controlling integrated processes, within aggregates from aerated (exterior) environments.

Using a combination of a synthetic aggregate experiments and reactive transport modeling, we reveal that microscale variation in As and Fe speciation and distribution develops within structured media even when advective flow remains aerated. While the exterior of aggregate remains oxic, anoxia develops within the aggregates where As(V) and Fe(III) reduction transpire. Consequently, the proportions of As(III) and magnetite increase progressively toward the aggregate interior. Reactive transport simulations confirm the sharp decrease in oxygen concentration and gradual increase in Fe(II) concentration from the aggregate exterior toward the aggregate interior. Further, a portion of As(III) and Fe(II) produced within the aggregate migrates toward the advective front and precipitates along the aggregate exteriors upon contact with oxygen, resulting in the accumulation of As and Fe on the aggregate exterior proximal to preferential flow paths.

* Corresponding author phone: (650)-723-5238; fax: (650)-725-2199; e-mail: fendorf@stanford.edu.
† Stanford University.
‡ The University of British Columbia.

Materials and Methods

Aggregate Construction. Aggregates of As(V)-bearing ferrihydrite-coated sand were made under aerated conditions. Two-line ferrihydrite was synthesized (*17*), mixed with quartz sand. Sand (250 g) was then reacted with sterile basal salt medium (BSM) containing 0.26 μM NaH_2PO_4 to preload phosphate for microbial function. The BSM contained 10 mM PIPES, 2.7 mM KCl, 0.3 mM $MgSO_4$, 7.9 mM NaCl and 0.4 mM $CaCl_2 \cdot 2H_2O$, and its pH was adjusted to 7.1 and autoclaved. After 3 days of reaction, the BSM with phosphate was replaced with a BSM containing 2.5 mM $Na_2HAsO_4 \cdot 7H_2O$ and allowed to react another 3 days; the solids were then washed twice with the BSM. The final As(V) loading of sand was 0.053 mol As(V)/mol Fe, which is 52% of Langmuir maximum (*9*).

Shewanella sp. ANA-3 was grown aerobically in tryptic soy broth and harvested as described previously (*13*). *Shewanella* sp. ANA-3 is a facultative anaerobe that is capable of aerobic respiration coupled to lactate or acetate oxidation, and dissimilatory As(V) and Fe(III) reduction couple to incomplete oxidation of lactate (*18*).

As(V)-bearing ferrihydrite-coated sand was homogeneously inoculated with *Shewanella* sp. ANA-3 to a density of 7×10^8 cells g^{-1} dry sand and fused using agarose (2.5 g agarose kg^{1-} sand) into 2.5 cm (ID) spheres. The aggregates had a dry bulk density of 1.19 g cm^{-3} and a porosity of 0.58 (*19*).

Redistribution of As and Fe within Aggregates under Aerated Flow. A single aggregate was placed in the center of a flow-through reactor, which was constructed from polycarbonate (L = 3.7 cm, ID = 5.1 cm) and had 0.2 μm filters embedded at each end (Supporting Information (SI) Figure SI-1). Flow of aerated BSM containing 3.8 mM lactate, 17.8 μM NH_4Cl and Wolfe's mineral solution (1 mL L^{-1}) (*20*) was initiated at 1 mL h^{-1} from the bottom. Reactors were continuously purged with sterile air. Effluent was collected by pumping (1 mL h^{-1}) from the tops of the reactors. Replicate aggregate reactors were terminated after 10 and 20 days. Solid phase measurements are based on destructive sampling of a single aggregate at each time interval.

Upon experiment termination, aggregates were harvested and sectioned into three concentric layers, exterior "E" (0−3.5 mm from the aggregate surface), midsection "M" (3.5−7.5 mm) and interior "I" (7.5−12.5 mm); sectioning was used to obtain coarse spatial information but was not predicated on specific redox zones. The solids from various sections were then used for bulk X-ray absorption spectroscopic (XAS) analysis, cell counts, and digestion with 6 M HCl. Radial slices of the aggregates were obtained for micro-X-ray fluorescence (μ-XRF) mapping and μ-XAS analysis.

Analysis. Solid phase total Fe and As were determined by analyzing 6 M HCl digested samples. Average concentrations of initial solid phase Fe and As were 129 ($\pm$2.81) mmol Fe kg^{-1} sand and 6.80 ($\pm$0.325) mmol As kg^{-1} sand. Due to addition of exfoliated Fe (hydr)oxides from the sand during transfer to acid digest vessels, total Fe and As values may be slightly over determined.

Cell counts were accomplished by first removing cells from the solids using 10 mM sodium pyrophosphate at pH 7 with sonication. Cells were then fixed with formaldehyde, stained with DAPI (4′,6-diamidino-2-phenylindole), vacuum filtered onto a polycarbonate filter and counted using epifluorescence microscopy.

Bulk X-ray absorption spectroscopic (XAS) was conducted on beamline 11−2 at the Stanford Synchrotron Radiation Lightsource (SSRL), using a similar method to that described previously (*11, 13*). Homogeneous As−Fe layers were prepared by vacuum filtration of sonicated As−Fe phases onto cellulose nitrate filters, and sealed in two layers of Kapton tape. A double crystal Si(220)

monochromator was used for energy selection. Solid-phase speciation of Fe was accomplished using the extended portion (EXAFS) of the Fe K-edge spectrum; scans were obtained from 100 eV below to 1000 eV above the Fe K-edge at 7111 eV. Data reduction and linear combination k^3-weighted EXAFS spectral fitting were performed using the SIXPACK interface to IFFEFIT (*21*). Briefly, Fe fluorescence spectra were normalized, and the backscattering contribution was isolated by subtracting a spline function. Resulting data were then converted from energy (eV) to k space ($Å^{-1}$), and k^3 weighted. Linear-combination fitting of the reduced Fe spectra was performed from 3 to 14 $Å^{-1}$, while minimizing reduced chi square values. Ferrihydrite and magnetite were used as reference compounds for fittings based on their likelihood of being a reaction product (*11, 13*), as well as observations using scanning electron microscopy (SEM) (SI Figure SI-3). Quantitative determination of As(V) and As(III) in the reacted solids was accomplished using the near-edge portion (XANES) of the As K-edge spectrum; scans were collected from 240 eV below to 430 eV above the As(V) K-edge of 11874 eV. Linear combination XANES spectral fitting was performed using SIXPACK to deduce the proportion of As(V) to As(III) while minimizing reduced chi square values. Arsenic(V) and As(III) adsorbed on ferrihydrite were used as fitting standards.

Micro-XAS/XRF data were collected on beamline 2−3 at SSRL and beamlime 10.3.2 at the Advanced Light Source (ALS). Aggregate slices were dried and cured in EPOTEK301−2FL resin under anoxic conditions. Sample was then sectioned to 30 μm thicknesses, and mounted on a quartz slide. Arsenic μ-XANES data were collected and quantitatively analyzed for As(V) and As(III) as described in bulk data analysis. Averages of As μ-XANES data in all sections (E, M, I) matched well with bulk As XANES data, suggesting that redox reaction of As in resin was minimum during data collection. Total Fe and Si fluorescence were recorded simultaneously. The aggregates were mapped from the exterior to interior (12.5 × 0.5 mm) at 3 energy values (11871, 11875, and 11880 eV) with 5 or 12 μm step sizes. Arsenic speciation across the aggregates was determined by the XANES imaging subroutine SMAK—a subroutine of SIXPAK (*22*). Briefly, linear least-squares regression was performed on each data point within the maps, using As(III) and As(V) adsorbed ferrihydrite as standards, to construct 2-D images of As speciation across the aggregates.

Reactive Transport Simulations. Numerical modeling was performed using MIN3P, a general purpose reactive transport code capable of coupling advective-diffusive flow, aqueous and heterogeneous (bio)geochemical reactions, and solid phase transformations. Details of the general model are thoroughly described by Mayer et al (*23*).

The biogeochemical processes operating within our experiments were translated into a biogeochemical reaction network constrained within a set of physical parameters governing hydraulic flow, including advective and diffusive mass transfer (Table 1). These simulated (bio)geochemical reactions are constrained within a three-dimensional physical framework consisting of a low K spherical aggregate (1.25 cm radius aggregate) surrounded by an open cylindrical channel (2.5 cm radius) dominated by advective flow (SI Figure SI-1); mass transfer to the spherical aggregate is therefore controlled by diffusion, as previously shown by Pallud et al (*24*). Further information regarding the modeling approach is presented in the SI.

Results

Experimental Observation. Within the aggregate, Fe and As content and speciation changed temporally and spatially relative to the initial condition. The total solid-phase Fe

TABLE 1. Reaction Network Used within the Reactive Transport Model

inter-aqueous reactions		log K
$4Fe^{3+} + C_3H_5O_3^- + 2H_2O \rightarrow 4Fe^{2+} + CO_3^{2-} + 5H^+ + CH_3COOH$	(1)	_[a]
$O_{2(aq)} + C_3H_5O_3^- \rightarrow CO_3^{2-} + H^+ + CH_3COOH$	(2)	_[a]
$2H_3AsO_4 + C_3H_5O_3^- \rightarrow 2H_3AsO_3 + CO_3^{2-} + H^+ + CH_3COOH$	(3)	_[a]
$Fe^{2+} + 0.25O_2 + H^+ \rightarrow Fe^{3+} + 0.5H_2O$	(4)	_[a]
Mineral Dissolution/Precipitation		
$2Fe^{3+} + Fe^{2+} + 4H_2O \rightarrow Fe_3O_{4(s)} + 8H^+$	(5)	$-3.73\ 7^{[b]}$
$Fe^{3+} + 3H_2O \rightarrow Fe(OH)_{3(s)} + 3H^+$	(6)	$1.000^{[c]}$
Arsenic Adsorption/Desorption[d]		
$H_3AsO_4 + \equiv FeOH_{(w)} \rightarrow H_2O + \equiv FeH_2AsO_{4(w)}$	(7)	15.030
$H_3AsO_3 + \equiv FeOH_{(w)} \rightarrow H_2O + \equiv FeH_2AsO_{3(w)}$	(8)	6.530

[a] Kinetically limited irreversible reactions. [b] Robie and Waldbaum (27). [c] Within range of values presented by Cornell and Schwertmann (28). [d] Values calibrated from abiotic desorption data, see SI for details.

TABLE 2. Solid Phase Characteristics of the Aggregate Exterior "E" (0–3.5 mm), Midsection "M" (3.5–7.5 mm), and Interior "I" (7.5–12.5 mm) of Aggregates (ID 2.5 cm) Reacted with *Shewanella* sp. ANA-3 under Aerated Advecting Flow

	[a]Total As (μmol)	[b]simulated total As (μmol)	[c]total Fe (μmol)	[d]simulated total Fe (μmol)	[e]As/Fe molar ratio	[f]cell density (cells g^{-1} sand)
Initial						
E	41.5 (1.98)	41.5	787 (17.1)	787	0.0527	7.0×10^8 (7.5×10^7)
M	20.5 (0.98)	20.5	388 (8.46)	388	0.0527	7.0×10^8 (7.5×10^7)
I	4.22 (0.20)	4.22	80.0 (0.62)	80	0.0527	7.0×10^8 (7.5×10^7)
total	66.2 (3.16)	66.2	1260 (27.3)	1255		
10 Days						
E	39.1	41.5	885	817	0.0442	8.0×10^8 (3.1×10^8)
M	20.5	20.5	388	325	0.0528	8.0×10^8 (3.7×10^8)
I	4.22	4.22	78.1	69	0.0540	8.3×10^8 (1.6×10^8)
total	63.8	66.2	1350	1211		
20 Days						
E	37.9	41.5	872	872	0.0435	8.5×10^8 (2.6×10^8)
M	19.9	20.5	346	280	0.0575	5.6×10^8 (8.4×10^7)
I	4.34	4.22	76.3	61	0.0569	5.7×10^8 (1.6×10^8)
total	62.2	66.2	1295	1214		
52 Days						
E	46.4	40.3	1159	1068	0.0400	8.5×10^8 (1.1×10^8)
M	16.5	19.3	286	129	0.0575	4.6×10^8 (8.8×10^7)
I	4.17	3.97	52.7	38	0.0795	1.2×10^8 (1.9×10^7)
total	67.1	63.5	1498	1235		

[a] Mass of solid phase in each sections of the aggregate was calculated from 6 M HCl digestion. The exterior (E) had 6.1 g, the midsection (M) had 3.0 g, and the interior (I) had 0.6 g of ferrihydrite coated sand based on the bulk density of aggregate (1.19 g cm^{-3}). Values in parentheses are standard deviation of triplicate values. Arsenic and Fe concentrations normalized by total mass are reported in SI Table SI-3. [b] Simulated mass of As computed by the reactive transport modeling. [c] Mass of solid phase Fe in each sections of aggregate, calculated similarly to the mass of As. Values in parentheses are standard deviation of triplicate values. [d] Simulated mass of Fe computed by the reactive transport modeling. [e] As/Fe molar ration based on the mass of As and Fe on solids (a). [f] Determined by DAPI staining. Values in parentheses represent standard deviation from counting in at least 10 fields of view.

content of the aggregate exterior increased by 372 μmol relative to the initial concentration over 52 days of reaction (Table 2), and the μ-XRF analysis confirmed the accumulation of Fe on sand grains within the first 3 mm of the aggregate exterior (Figure 1). In contrast to the aggregate exterior, the midsection lost 42 μmol Fe after 20 days and 102 μmol Fe after 52 days. The interior lost 3.7 μmol Fe after 20 days and 27 μmol Fe after 52 days relative to the initial Fe content (Table 2).

On the basis of Fe EXAFS analyses, the aggregate exterior remained as ferrihydrite (Table 3 and SI Figure SI-4), consistent with the bright orange color (Figure 1). Iron EXAFS
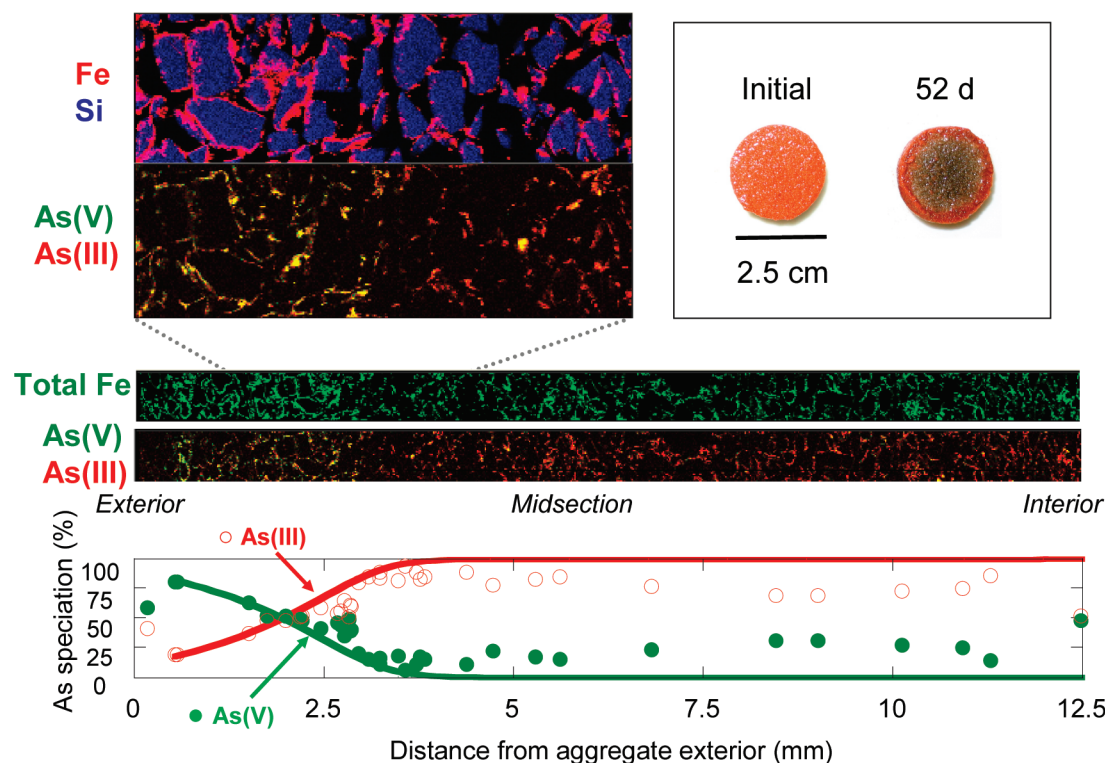
FIGURE 1. Photograph (top right), X-ray fluorescence maps (middle and top left), and As species distribution (data = circles and simulation = solid lines; bottom panel) for aggregate cross section after 52 days of reaction. The summary of μ-XANES fitting results are provided in SI Table SI-4.

TABLE 3. Solid Phase As and Fe Speciation of Aggregate Exterior "E" (0–3.5 mm), Midsection "M" (3.5–7.5 mm), and Interior "I" (7.5–12.5 mm) of Aggregates (ID 2.5 cm) Reacted With *Shewanella* sp. ANA-3 under Aerated, Advective Flow

|	[a]As speciation (mol-%)		[b]simulated As speciation (mol-%)		[c]dominant Fe mineralogy (mol-%)		[d]simulated dominant Fe mineralogy (mol-%)	
	As(V)	As (III)	As(V)	As (III)	ferrihydrite	magnetite	ferrihydrite	magnetite
0 Days								
E	100	0	100	0	100	0	100	0
M	100	0	100	0	100	0	100	0
I	100	0	100	0	100	0	100	0
10 Days								
E	43	57	89	11	97	0	99	1[e]
M	34	66	34	66	96	0	95	5
I	37	63	22	78	96	0	94	6
20 Days								
E	42	58	77	23	98	0	98	2[e]
M	16	84	0	100	90	10	92	8
I	16	84	0	100	93	7	91	9
52 Days								
E	46	54	48	52	100	0	97	3[e]
M	12	88	0	100	91	9	80	20
I	8	92	0	100	85	15	80	20

[a] Determined with As XANES linear combination fitting. Data is shown in SI Figure SI-5. [b] Simulated As speciation computed by the reactive transport modeling. [c] Determined with Fe EXAFS linear combination fitting. Data and fits are shown in SI Figure SI-4. [d] Simulated Fe mineralogy computed by the reactive transport modeling. [e] Value is below confidence limit.

analyses and SEM observations show that magnetite content increased toward the aggregate interior, resulting in darkening of the solids (Table 3, Figure 1, and SI Figure SI-4). Although magnetite was not detected after 10 days, 10 mol-% Fe in midsection and 7 mol-% in the interior of the aggregate were detected as magnetite after 20 days. After 52 days, 9 mol-% in midsection and 15 mol-% in the interior were detected as magnetite after 52 days (SI Table 3 and SI Figure

SI-4). Magnetite crystals were observed under SEM in the interior of the aggregate after 52 days (SI Figure SI-3).

Changes in As distribution and speciation were also observed within the aggregate. The aggregate exterior lost 2.4 μmol As after 10 days and 3.5 μmol As after 20 days, but the As content in the midsection and interior of aggregate was unchanged during this period (Table 2). After 52 days, the As content increased by 7.3 μmol in the aggregate exterior

aggregate exterior   aggregate interior
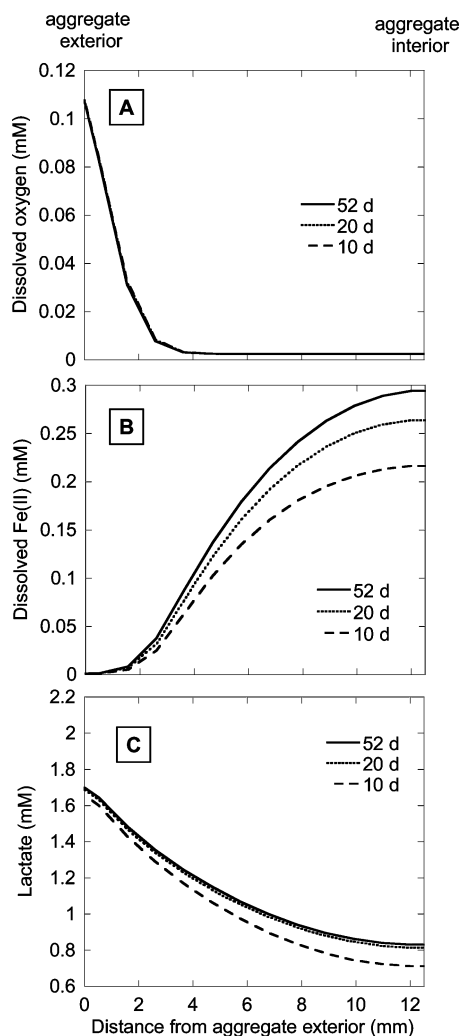
FIGURE 2. Reactive transport simulation results of dissolved (A) oxygen, (B) Fe(II), and (C) lactate as a function of a distance from aggregate exterior.

relative to its initial content despite the decrease in As content during the initial 20 days. The As content decreased by 4.0 μmol in the midsection but remained virtually identical in the interior after 52 days.

An abrupt change in solid-phase As speciation was observed within the aggregate. μ-XANES and μ-XRF analysis show the dominant As species changed abruptly from As(V) to As(III) 3 mm in from the outer surface after 52 days (Figure 1). Bulk As XANES results were consistent with μ-XANES and μ-XRF analysis, and show that the proportion of As(V) was highest at the exterior and decreased toward the aggregate interior (Table 3 and Figure 1). The observed transition of dominant As species within the aggregate became pronounced over time. Based on bulk XANES measurement, As speciation was relatively constant within the aggregate exterior during the course of the experiment (Table 3). However, the proportion of As(III) increased over time within the interior regions as Shewanella continuously reduced As(V) (Table 3).

Cell density was highest in the aggregate exterior (8.5 ± 1.1 × 10^8 cells g^{-1} sand) and progressively decreased in the midsection (4.6 ± 0.9 × 10^8 cells g^{-1} sand) and interior (1.2 ± 0.2 × 10^8 cells g^{-1} sand) over 52 days (Table 2). Higher bacterial density at the aerated exterior is likely due to the presence of molecular oxygen (Figure 2A), which declines, along with bacterial counts, when progressing from the exterior to interior region of the aggregate.

Reactive Transport Modeling. Reactive transport modeling was performed to quantitatively simulate As and Fe transformation/migration and electron flow, and to compute chemical gradients within the aggregate as a function of time and space. Measured solid phase Fe and As concentrations, Fe mineralogy, and As speciation (Tables 2 and 3) were used to constrain model reactions (Table 1). A detailed explanation of the model calibration is provided in the SI.

Model simulations captured the main aspect of As and Fe distribution and speciation throughout the aggregate—both the mass and speciation of solid phase As and Fe were reproduced quantitatively temporally and spatially (Tables 2 and 3 and Figure 1). Based on the projected consumption of oxygen through Fe(II) oxidation and consumption by Shewanella, reactive transport simulations illustrate a gradual decrease in oxygen concentration from near-equilibrium with the atmosphere (0.11 mM) at the aggregate surface, to near-complete depletion 3.5 mm into the aggregate (Figure 2A). The predicted oxygen spatial gradient remained constant for the duration of the experiment (52 days) and is consistent with the presence of bright orange rim (absence of magnetite) and the greater proportion of As(V) at the exterior (~3 mm) of the aggregate (Figure 1).

The presence of appreciable dissolved oxygen limits Fe(III) reduction by dissimilatory metal reducing bacteria (5). Additionally, abiotic oxidation of Fe(II) by oxygen is rapid at circum-neutral pH, and will transpire within the exterior where oxygen is present and where dissolved Fe(II) may migrate via diffusion from the anoxic aggregate interior. Accordingly, simulations illustrate the absence of dissolved Fe(II) at aggregate surface (0−3 mm) throughout the experiment. Beyond the zone of oxygen depletion, Fe(III) and As(V) reduction are utilized in microbial respiration for lactate oxidation—results consistent with experimental observation (Table 3 and Figure 1). As a consequence, Fe(II) concentration gradually increased toward the center of the aggregate (Figure 2B) where oxygen is depleted. Additionally, elevated dissolved Fe(II) concentrations toward the aggregate center are consistent with the formation of magnetite and darkening of the solids (Figure 2B); a lack of Fe(II) in the oxygenated exterior (0−3 mm) is consistent with an absence of magnetite in this region (Table 3).

Based on model simulations, lactate concentrations progressively decreased from 1.7 mM at the surface to 0.7 mM at the center of the aggregate after 10 days (Figure 2C) and remained near this value until the end of the experiment (Figure 2C). Furthermore, lactate was predicted to diffuse rapidly into the aggregate upon introduction to the groundwater solution; after ~1 day, simulations illustrate that lactate was not a limiting reactant anywhere in the model domain, consistent with the rapid microbial reduction of Fe(III) and As(V).

Discussion

Intra-Aggregate Redistribution and Transformation of As and Fe. Intra-aggregate redistribution of Fe and As occurs due to redox gradients resulting from progressive oxygen consumption from the exterior toward the interior. Within the aggregate exterior, Shewanella aerobically respires at a rate exceeding that of oxygen diffusion (Figure 2A). As a result, As(V) and Fe(III) serve as the electron acceptors for Shewanella respiration, leading to the formation of As(III) and Fe(II) in the aggregate interior. Internal redistribution of As and Fe thus results due to spatial distribution of As and Fe reduction and oxidation; reduction transpiring in the aggregate midsection and interior and oxidation within the aggregate exterior. Although minimal for the first 20 days, changes in As and Fe distribution are observed by 52 days. Three discrete zones of As and Fe emerged within the aggregate by 52 days: accumulation of As and Fe in the
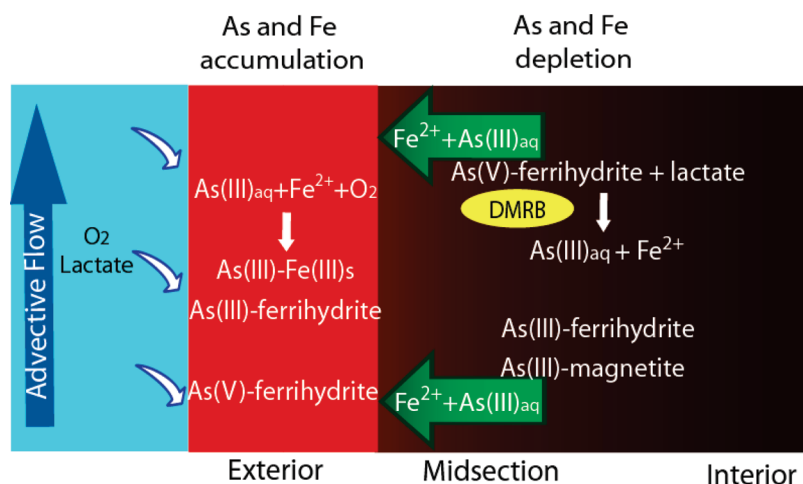
FIGURE 3. Schematic of reactions involving As and Fe within the aggregate. DMRB refers to dissimilatory metal reducing bacteria.

exterior, depletion of As and Fe in the midsection, and no change in As, despite the loss of Fe, in the interior section.

During the initial 20 days, As is depleted from the exterior region (Table 2), likely as a result of a labile fraction being removed in the proximal advecting solute. This is consistent with an outer-sphere complex noted by Catalano et al. (25) and our previous results (9). Initial loss of As from the aggregate exterior is also due to insufficient production or supply of Fe(II) from the aggregate interior to induce retention of As within the surface structure of newly formed Fe(III) hydroxides (in contrast to results after 52 days). As the reaction progresses, increasing quantities of Fe(II) from the interior regions migrated to the exterior, which sequestered As during oxidative precipitation of Fe(III). The experimental findings are well described by the reactive transport simulation, which illustrate increased migration of Fe(II) from the midsection and interior of the aggregate to the exterior over time (Table 2). Only 85 μmol of Fe accumulated in the exterior after 20 days, compared to 372 μmol of Fe after 52 days (Table 2).

During reaction progression, ferrihydrite begins transforming to magnetite with increased Fe(II) concentrations in the midsection and interior of the aggregates, which further consumes Fe(II) and limits diffusion into the exterior region. After 20 days, 10 and 7 mol-% magnetite is found (Table 3), which corresponds to 12 and 2 μmol Fe(II) within midsection and interior of the aggregate, respectively. Continuous production of Fe(II) within the aggregates over 52 days leads first to secondary mineral formation and secondarily to diffusion toward the exterior of the aggregate (Figure 2B).

After 52 days, both As and Fe accumulated in the exterior region of the aggregate, illustrating a substantial internal redistribution of both elements; the processes leading to the redistribution are summarized schematically in Figure 3. Arsenic and Fe lost from the internal regions redistributes to the oxygenated exterior. Migration of Fe toward the exterior results from reductive dissolution in the interior and oxidative precipitation of Fe(III) hydroxides in the exterior, maintaining a Fe(II) diffusion gradient (as shown in Figure 3). Arsenic(III) accumulation in the exterior then results due to incorporation within the precipitating Fe(III) hydroxides.

An abrupt change in the dominant As species from As(V) to As(III) occurs ca. 3 mm from the aggregate exterior and coincides with a zone of Fe accumulation, both of which are consistent with reactive transport simulations showing oxygen is maintained in the outer rim (0−3 mm) of the aggregate. Unlike Fe(II), As(III) oxidation by molecular oxygen is slow (26) and thus some As(III) is likely to remain within the oxygenated zone; however, As(V) reduction would be limited in this region. Within the midsection, a diffusion gradient established from Fe(III) precipitation and con-

comitant sorption of As(III) in the exterior results in depletion of As. The midsection lost 4 μmol As and 102 μmol Fe, and the proportion of As(III) increased to 88% after 52 days.

In the aggregate interior region, Fe loss is prominent; however, the As content did not change, largely due to magnetite formation and resulting As sequestration. Arsenic sequestration during reductive transformation of ferrihydrite to magnetite has also been observed during column and batch experiments (10, 11, 13). Temporal increases in magnetite within aggregate midsection and interior are likely due to gradual increase in pore-water Fe(II) concentration, illustrated by the reactive transport simulation (Figure 2B). As a result of Fe(II) diffusion from the interior coupled with magnetite formation, the As/Fe molar ratio increases markedly from an initial value of 0.053 to a value of 0.08 after 52 days of reaction (Table 2).

Role of Anaerobiosis within Mass-Transfer Limited Zones. Physical heterogeneity common to soils and sediments will have a strong influence on the biogeochemical conditions controlling the fate and transport of As (and, by association, other elements). Even within aerated soils, anaerobiosis within aggregates, or any diffusion-controlled environment, will result in As(V) and Fe(III) reduction. As a consequence, steep redox gradients result and cause changes in the distribution and speciation of these elements. An increased As/Fe molar ratio within the aggregate interior also suggest that cessation of magnetite production will lead to As(III) migration toward the aggregate exterior. Owing to oxygenated conditions in the outer rim of the aggregate, Fe(III) hydroxide precipitates and results in concomitant As sequestration. Thus, As accumulates near the advective flow boundary, a result of differential redox conditions. Importantly, the build-up of As on Fe(III) (hydr)oxides in the outer-rim of the aggregate could accelerate As release upon the onset of full anaerobic conditions (i.e., a transition to anaerobic conditions within the preferential flow path). Ultimately, site-specific chemical, biological, and physical complexities must be considered to understand and predict As fate and transport within physically complex environments such as soils and sediments.

Acknowledgments

this research were carried out at SSRL and ALS, user facilities supported by the Department of Energy, Office of Basic Energy Sciences.

Supporting Information Available

Detailed method of reactive transport modeling, schematic illustrations of the aggregate reactor (Figure SI-1), the mesh used in the model (Figure SI-2), SEM images of aggregate solids (Figure SI-3), and Fe EXAFS data and fits (Figure SI-4), As XANES data and fits (Figure SI-5), additional model stimulation results (Figure SI-6), rate expressions for reactions used in simulation (Table SI-1), kinetic and thermodynamic values used in the model (Table SI-2), and solid-phase concentrations of As and Fe normalized to mass (Table SI-3), and the summary of As μ-XANES analysis (Table SI-4) are provided. This material is available free of charge via the Internet at http://pubs.acs.org.

Literature Cited

(1) Smedley, P. L.; Kinniburgh, D. G. A review of the source, behaviour and distribution of arsenic in natural waters. *Appl. Geochem.* **2002**, *17* (5), 517–568.

(2) Masue, Y.; Loeppert, R. H.; Kramer, T. A. Arsenate and arsenite adsorption and desorption behavior on coprecipitated aluminum:iron hydroxides. *Environ. Sci. Technol.* **2007**, *41* (3), 837–842.

(3) Manning, B. A.; Goldberg, S. Adsorption and stability of arsenic(III) at the clay mineral-water interface. *Environ. Sci. Technol.* **1997**, *31* (7), 2005–2011.

(4) Manning, B. A.; Goldberg, S. Arsenic(III) and arsenic(V) absorption on three California soils. *Soil Sci.* **1997**, *162* (12), 886–895.

(5) Lovley, D. R. Dissimilatory Fe(III) and Mn(IV) Reduction. *Microbiol. Rev.* **1991**, *55* (2), 259–287.

(6) Newman, D. K.; Ahmann, D.; Morel, F. M. M. A brief review of microbial arsenate respiration. *Geomicrobiol. J.* **1998**, *15* (4), 255–268.

(7) Raven, K. P.; Jain, A.; Loeppert, R. H. Arsenite and arsenate adsorption on ferrihydrite: Kinetics, equilibrium, and adsorption envelopes. *Environ. Sci. Technol.* **1998**, *32* (3), 344–349.

(8) Dixit, S.; Hering, J. G. Comparison of arsenic(V) and arsenic(III) sorption onto iron oxide minerals: Implications for arsenic mobility. *Environ. Sci. Technol.* **2003**, *37* (18), 4182–4189.

(9) Tufano, K. J.; Reyes, C.; Saltikov, C. W.; Fendorf, S. Reductive processes controlling arsenic retention: Revealing the relative importance of iron and arsenic reduction. *Environ. Sci. Technol.* **2008**, *42* (22), 8283–8289.

(10) Coker, V. S.; Gault, A. G.; Pearce, C. I.; van der Laan, G.; Telling, N. D.; Charnock, J. M.; Polya, D. A.; Lloyd, J. R. XAS and XMCD evidence for species-dependent partitioning of arsenic during microbial reduction of ferrihydrite to magnetite. *Environ. Sci. Technol.* **2006**, *40* (24), 7745–7750.

(11) Kocar, B. D.; Herbel, M. J.; Tufano, K. J.; Fendorf, S. Contrasting effects of dissimilatory iron(III) and arsenic(V) reduction on arsenic retention and transport. *Environ. Sci. Technol.* **2006**, *40* (21), 6715–6721.

(12) Herbel, M.; Fendorf, S. Biogeochemical processes controlling the speciation and transport of arsenic within iron coated sands. *Chem. Geol.* **2006**, *228* (1−3), 16–32.

(13) Tufano, K. J.; Fendorf, S. Confounding impacts of iron reduction on arsenic retention. *Environ. Sci. Technol.* **2008**, *42* (13), 4777–4783.

(14) Tokunaga, T. K.; Wan, J. M.; Hazen, T. C.; Schwartz, E.; Firestone, M. K.; Sutton, S. R.; Newville, M.; Olson, K. R.; Lanzirotti, A.; Rao, W. Distribution of chromium contamination and microbial activity in soil aggregates. *J. Environ. Qual.* **2003**, *32* (2), 541–549.

(15) Sexstone, A. J.; Revsbech, N. P.; Parkin, T. B.; Tiedje, J. M. Direct measurement of oxygen profiles and denitrification rates in soil aggregates. *Soil Sci. Soc. Am. J.* **1985**, *49* (3), 645–651.

(16) von Fischer, J. C.; Hedin, L. O. Separating methane production and consumption with a field-based isotope pool dilution technique. *Global Biogeochem. Cycles* **2002**, *16* (3), XXX.

(17) Schwertmann, U.; Cornell, R. M., *Iron Oxides in the Laboratory: Preparation and Characterization*; VCH: New York, 1991; p137.

(18) Saltikov, C. W.; Wildman, R. A.; Newman, D. K. Expression dynamics of arsenic respiration and detoxification in Shewanella sp strain ANA-3. *J. Bacteriol.* **2005**, *187* (21), 7390–7396.

(19) Pallud, C.; Masue-Slowey, Y.; Fendorf, S. Aggregate-scale spatial heterogeneity in reductive transformation of ferrihydrite resulting from coupled biogeochemical and physical processes. *Geochim. Cosmochim. Acta* **2010**, *74* (10), 2811–2825.

(20) Balch, W. E.; Fox, G. E.; Magrum, L. J.; Woese, C. R.; Wolfe, R. S. Methanogenss reevaluation of a unique biological group. *Microbiol Rev* **1979**, *43*, 260–296.

(21) Webb, S. M. Sixpack: A graphical interface for XAS analysis using IFEFFIT. *Phys. Scr.* **2005**, *T115*, 1011–1014.

(22) Webb, S. M. SMAK: Sam's microprobe analysis kit. http://ssrl.slac.stanford.edu/~swbb/smak.htm, 2008.

(23) Mayer, K. U.; Frind, E. O.; Blowes, D. W. Multicomponent reactive transport modeling in variably saturated porous media using a generalized formulation for kinetically controlled reactions. *Water Resour. Res.* **2002**, *38* (9), XXX.

(24) Pallud, C.; Kausch, M.; Fendorf, S.; Meile, C. Spatial patterns and modeling of reductive ferrihydrite transformation observed in artificial soil aggregates. *Environ. Sci. Technol.* **2010**, *44* (1), 74–79.

(25) Catalano, J. G.; Zhang, Z.; Park, C. Y.; Fenter, P.; Bedzyk, M. J. Bridging arsenate surface complexes on the hematite (012) surface. *Geochim. Cosmochim. Acta* **2007**, *71* (8), 1883–1897.

(26) Inskeep, W. P.; McDermott, T. R.; Fendorf, S., Arsenic (V)/(III) cycling in soils and natural water: Chemical and microbiological processes. In *Environmental Chemistry of Arsenic*; Frankenberger, W. T., Ed.; Marcel Dekker: New York, 2002; pp 183−215.

(27) Robie, R. A.; Waldbaum, D. R. *Thermodynamic Properties of Minerals and Related Substances at 298.15K (25.0C) and One Atmosphere (1.013 bar) Pressure and at Higher Temperatures*, 1259; U.S. Geological Survey: Reston, VA, 1968.

(28) Cornell, R. M., Schwertmann, U. *The Iron Oxides*; 2nd ed.; Wiley-VCH: Druckhaus Darmstadt, 2003.

ES1027663